Large tunneling magnetoresistance in perpendicularly magnetized magnetic tunnel junctions using Co$_3$Mn/Mo/CoFeB multilayer

Tatsuya Yamamoto,[1, *] Tomohiro Ichinose,[1] Jun Uzuhashi,[2] Takayuki Nozaki,[1]

Tadakatsu Ohkubo,[2] Kay Yakushiji,[1] Shingo Tamaru,[1] and Shinji Yuasa[1]

[1]*National Institute of Advanced Industrial Science and Technology (AIST),*

Research Center for Emerging Computing Technologies, Tsukuba, Ibaraki 305-8568, Japan

[2]*National Institute for Materials Science (NIMS), Tsukuba, Ibaraki 305-0047, Japan*

(Dated: January 12, 2023)

Abstract

We study the magnetic and electrical transport properties of magnetic tunnel junctions (MTJs) consisting of a Co$_3$Mn/Mo/CoFeB multilayer prepared using a mass-production-compatible magnetron sputtering system. The Co$_3$Mn/Mo/CoFeB multilayer sandwiched between two MgO layers exhibits remarkable perpendicular magnetic anisotropy, and a uniaxial magnetic anisotropy constant as large as 0.2 MJ/m^3 is achieved by optimizing the Co$_3$Mn layer thickness as well as the annealing temperature. The current-in-plane tunneling measurement reveals a large tunneling magnetoresistance of over 100% in perpendicularly magnetized MTJs. These experimental results indicate the applicability of Co$_3$Mn alloy for magnetic random access memory devices.

---

* yamamoto-t@aist.go.jp

I. INTRODUCTION

Magnetic tunnel junctions (MTJs) using perpendicularly magnetized ferromagnetic layers have been intensively studied to develop high-density and energy-efficient magnetic random access memory (MRAM) devices [1–4]. In terms of MRAM application, a large tunneling magnetoresistance (TMR) is also required to improve the signal-to-noise ratio for a high-speed data readout. Among various MTJ materials, CoFe-alloys/MgO multilayers are the most promising material combination that enables a large TMR of over 100% [5–7] as well as a large perpendicular magnetic anisotropy (PMA) [8–11]. These remarkable TMR and PMA in CoFe-alloy/MgO MTJs originate from the coherent spin-polarized tunneling through the (001)-oriented MgO barrier [12, 13] and large interfacial PMA due to the hybridization of Fe(Co) $3d$ and O $2p$ orbitals [14, 15], respectively. The use of an amorphous CoFeB film enables the fabrication of MTJs with a highly (001)-oriented MgO barrier on a polycrystalline electrode using mass-production-compatible magnetron sputtering processes [9–11]. The CoFeB-based perpendicularly magnetized MTJs (p-MTJs) are currently used for state-of-art MRAM memory cells. Continued development of MTJ materials remains necessary for next-generation MRAMs including those using spin-orbit torque (SOT) [16–18] and/or the voltage-controlled magnetic anisotropy (VCMA) effect [19–21] to further improve the energy efficiency.

The use of bcc FeCoMn ternary alloys is a new approach for developing high-TMR MTJs [22, 23]. The bcc FeCoMn is a metastable phase that can be obtained from epitaxial growth on single crystalline substrates such as GaAs(001) [24] and MgO(001) [25–27]. An intriguing property of the bcc FeCoMn is the large magnetic moment that even exceeds the Slater Pauling limit depending on the alloy composition [27]. This unusual feature comes from the large magnetic moment of Mn atoms, which ferromagnetically aligns to that of Fe and Co atoms. First-principles calculation revealed that the band structure of bcc Co_3Mn alloy near the Fermi level is similar to those of bcc Fe and Co, i.e., the Δ_1 state only exists for the majority spin band at the Fermi level [23]. Kunimatsu et al. experimentally demonstrated a large TMR ratio of over 200% in an epitaxial Co_3Mn/MgO/Co_3Mn MTJ prepared on a single crystalline MgO(001) substrate [23]. Therefore, the next step toward practical use is to achieve large PMA in sputter-deposited polycrystalline films. In this article, we evaluate the magnetic and electrical properties of MTJs consisting of an ultrathin (< 1 nm) Co_3Mn film

2

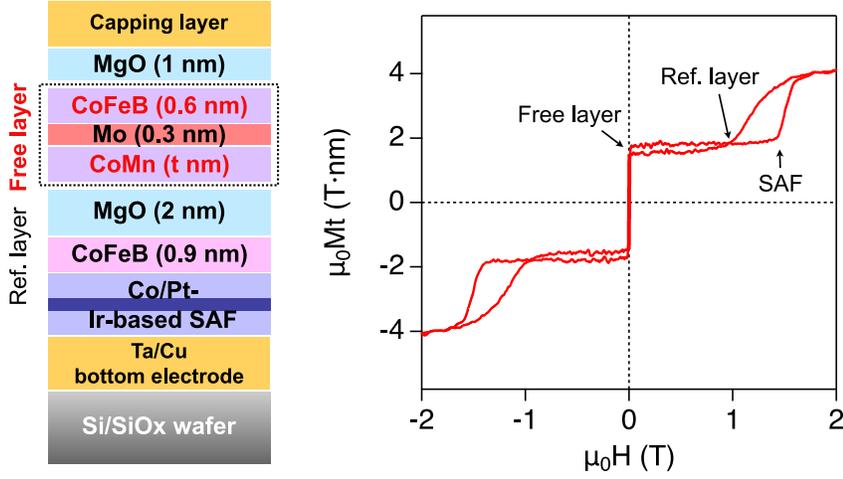FIG. 1. Schematic illustration of MTJ and representative magnetization curve obtained from MTJ consisting of a Co_3Mn (0.8 nm)/Mo (0.3 nm)/CoFeB (0.6 nm) multilayer annealed at 350°C. Magnetization curve was measured under application of out-of-plane magnetic field.

deposited using a mass-production-compatible magnetron sputtering system. The Co_3Mn ultrathin film deposited on an MgO barrier layer exhibits PMA, and p-MTJ films consisting of a Co_3Mn/Mo/CoFeB multilayer is deposited on 300-mm Si wafers with a polycrystalline electrode. TMR ratios of over 100% are also demonstrated by optimizing the Co_3Mn layer thickness and post annealing temperature.

II. EXPERIMENT

The MTJ films were prepared on 300-mm Si wafers with a 100-nm-thick thermally oxidized Si layer using an ultrahigh-vacuum magnetron sputtering system manufactured by Tokyo Electron Ltd (TEL-EXIM). After the deposition, the wafers were cut into 20×20 mm^2 square chips then annealed at $T_a = 200 - 380$°C for 1 h in a vacuum. Figure 1 shows a schematic of the MTJ stack along with a representative out-of-plane magnetization curve measured using a vibrating sample magnetometer (VSM). A strong antiferromagnetic coupling in the Co/Pt-based synthetic antiferromagnetic reference layer was obtained using an Ir spacer layer [28]. The Ta/Cu bottom electrode was used to evaluate the TMR as well as the resistance-area product of MTJ films by using the current-in-plane tunneling magnetoresistance (CIPT) technique [29]. The free layer consists of an MgO (2 nm)/Co_3Mn (t nm)/Mo

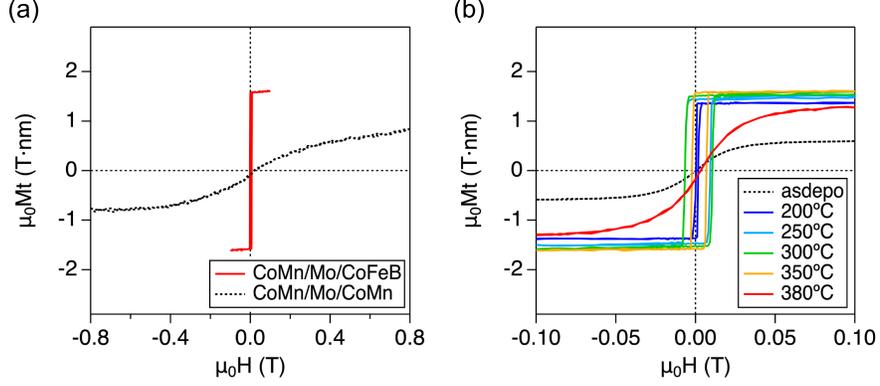FIG. 2. Out-of-plane minor magnetization curves representing magnetization process of free layer: (a) Co_3Mn (0.8 nm)/Mo (0.3 nm)/CoFeB (0.6 nm) and Co_3Mn (0.8 nm)/Mo (0.3 nm)/Co_3Mn (0.6 nm) free layers annealed at $T_a = 350°C$, and (b) Co_3Mn (0.8 nm)/Mo (0.3 nm)/CoFeB (0.6 nm) free layer annealed at various T_a.

(0.3 nm)/CoFeB (0.6 nm)/MgO (0.8 nm)/capping layer structure if not otherwise specified. The Mo spacer layer was chosen because Mo exhibits small intermixing with CoFe, and large PMA of over 0.3 MJ/m^3 has been reported for MgO/CoFeB/Mo/CoFeB/MgO multilayers [30].

A Co_3Mn alloy target was used for depositing the Co_3Mn thin films, and the sputtering rate of Co_3Mn, Mo and CoFeB were calibrated using X-ray fluorescence (XRF). The compositional ratio in the deposited Co_3Mn films was also determined by XRF to be Co 75.5 at.% versus Mn 24.5 at.%. To quantitatively evaluate the PMA in the MgO/Co_3Mn/Mo/CoFeB/MgO multilayer, we carried out vector network analyzer ferromagnetic resonance (VNA-FMR) measurement [31]. Scanning transmission electron microscopy (STEM), nano-beam electron diffraction (NBD), and energy dispersive X-ray spectrometry (EDS) were also carried out using FEI Titan G2 80-200 to investigate the nanostructural properties and atomic distribution of the MTJ. Thin foil specimens for the nanostructural analyses were prepared using a focused ion beam with a scanning electron microscopy system (FEI Helios G4UX) through a standard lift-out method.

III. RESULTS AND DISCUSSION

Figure 2(a) displays a minor magnetization curves obtained from the MTJ films consisting of Co_3Mn (0.8 nm)/Mo (0.3 nm)/CoFeB (0.6 nm) and Co_3Mn (0.8 nm)/Mo (0.3 nm)/Co_3Mn (0.6 nm) free layers. The MTJ films were annealed at $T_a = 350°C$. The saturation magnetization of the Co_3Mn/Mo/Co_3Mn free layer is considerably smaller than that of Co_3Mn/Mo/CoFeB free layer even if the difference in the saturation magnetization between bcc CoFe ($\sim$ 2.2 T [32]) and bcc Co_3Mn ($\sim$ 2.0 T [22, 26]) is taken into account. Therefore, it is expected that the fcc Co_3Mn phase with a much smaller magnetic moment is formed in the Co_3Mn/Mo/Co_3Mn free layer. It should be noted that the saturation field of the Co_3Mn/Mo/Co_3Mn free layer ($\sim$ 0.42 T) is smaller than the demagnetizing field ($\sim$ 0.68 T), which reveals finite positive PMA at the MgO/Co_3Mn interface. As shown in Fig. 2(a), the use of CoFeB instead of the upper Co_3Mn substantially enhances PMA and saturation magnetization, enabling a perpendicularly magnetized Co_3Mn layer. Therefore, it is considered that the formation of the fcc Co_3Mn phase is effectively prevented in the Co_3Mn/Mo/CoFeB multilayer.

Figure 2(b) displays minor magnetization curves obtained from the Co_3Mn (0.8 nm)/Mo (0.3 nm)/CoFeB (0.6 nm) free layer annealed at different T_a. Note that all these MTJ films including the as-prepared one underwent a thermal treatment at 80°C for about 3 min during the wafer-cut process. The as-prepared Co_3Mn/Mo/CoFeB free layer has an in-plane easy axis and exhibits a small saturation magnetization, indicating that the Co_3Mn layer is dominated by the paramagnetic phase(s). Interestingly, annealing at $T_a \geq 200°C$ leads to a remarkable enhancement in the saturation magnetization. This suggests that the Co_3Mn layer crystalizes into the ferromagnetic bcc phase upon annealing. The Co_3Mn/Mo/CoFeB free layer also exhibits perpendicular magnetization for $250°C \leq T_a \leq 350°C$. Annealing at a higher T_a degrades both the PMA and saturation magnetization.

Figure 3(a) displays a bright field (BF-)STEM image of the MTJ films consisting of the Co_3Mn (0.8 nm)/Mo (0.3 nm)/CoFeB (0.6 nm) multilayer after annealing at $T_a = 350°C$. The BF-STEM image as well as the NBD patterns [Fig. 3(b)] reveal the formation of (001)-oriented MgO layer and the partial crystallization of the Co_3Mn/Mo/CoFeB multilayer after annealing at $T_a = 350°C$. Although the crystalline structure of the Co_3Mn/Mo/CoFeB multilayer cannot be distinguished from the BF-STEM image and the NBD patterns shown in

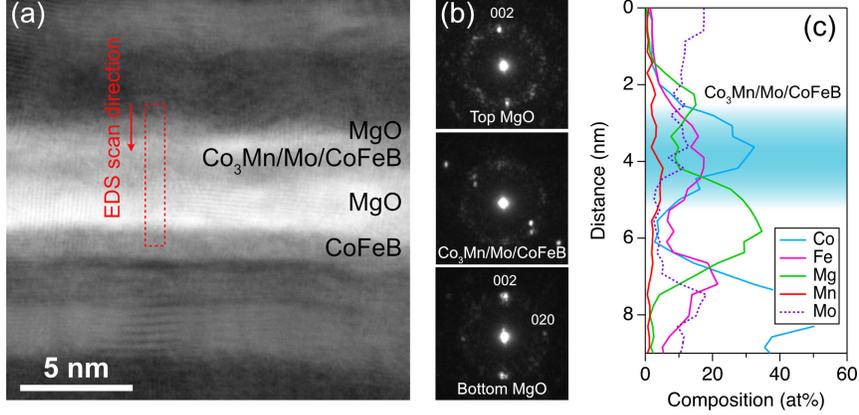FIG. 3. Nanostructural analysis results on Co$_3$Mn (0.8 nm)/Mo (0.3 nm)/CoFeB (0.6 nm) free layer annealed at $T_a = 350°$C: (a) BF-STEM image (b) NBD patterns, and (c) EDS elemental line profile.
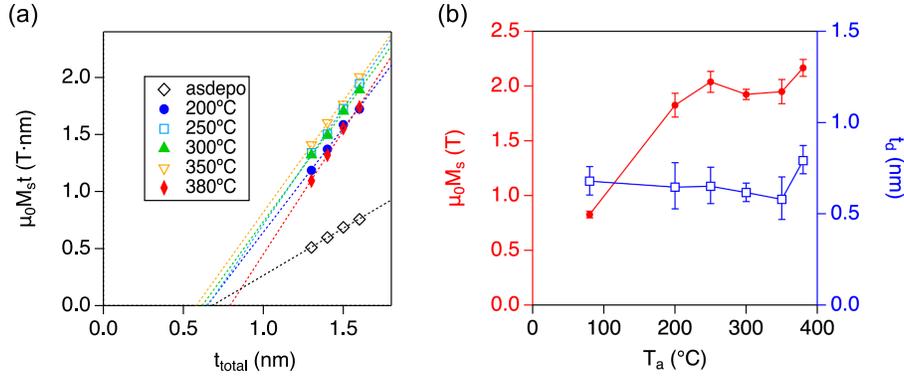

FIG. 4. Post annealing effect on Co$_3$Mn/Mo/CoFeB free layer: (a) Co$_3$Mn thickness dependence of $\mu_0 M_s t$, and (b) T_a dependence of $\mu_0 M_s$ and t_d. $t_{total} = t + 0.6$.

Fig. 3, the large saturation magnetization revealed from the VSM measurements suggests the bcc crystallization of Co$_3$Mn. Figure 3(c) displays the EDS elemental line profile obtained from the rectangle region drawn in Fig. 3(a) along the direction of the arrow. Due to the considerable film roughness, the atomic ratio at each position may contain a certain amount of uncertainty. However, it is noteworthy that we achieved perpendicular magnetization using a Co-rich ferromagnet, which is beneficial for improving the VCMA efficiency [33–35]. Note also that there is no significant change in the line profile of Mn atoms associated with the annealing, i.e., most Mn atoms remain on top of the MgO barrier layer. The interfacial Mn atoms can exhibit a large PMA as well as VCMA. [36].
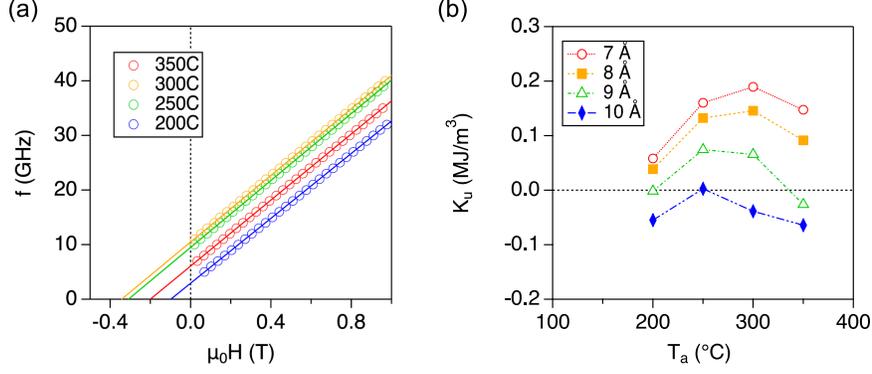
6

FIG. 5. VNA-FMR measurement results: (a) FMR frequency as function of applied out-of-plane field. (b) K_u values estimated from H_k and M_s values.

To estimate the saturation magnetization of Co_3Mn in our MTJ films, we evaluated the $\mu_0 M_s t_{total}$ values by varying the Co_3Mn thickness t in the MTJs, and the results are shown in Fig. 4(a). The total free layer thickness, t_{total}, is defined as the sum of the Co_3Mn and CoFeB thicknesses, i.e., $t_{total} = t + 0.6$ nm. The slope and t_{total}-intercept of linear fits to the experimental data correspond to the saturation magnetization $\mu_0 M_s$ and dead layer thickness in the $Co_3Mn/Mo/CoFeB$ stack t_d, respectively. Figure 4(b) summarizes the estimated values of $\mu_0 M_s$ and t_d as a function of T_a. Annealing at $T_a \geq 200°C$ remarkably enhanced the saturation magnetization, and $\mu_0 M_s$ values as large as 2.0 T were obtained for $250°C \leq T_a \leq 350°C$. For this T_a range, the t_d value was constant around 0.6 nm. These results suggest that the ferromagnetic (bcc) phase is stabilized in the Co_3Mn layer for $250°C \leq T_a \leq 350°C$. Annealing at $T_a = 380°C$ led to a slight increase in t_d, which can be explained by the formation of paramagnetic fcc phase [23] and interlayer atomic diffusion in the $Co_3Mn/Mo/CoFeB$ stack. These magnetic phase transition in Co_3Mn may be used to further improve the efficiencies of VCMA- and SOT-driven magnetization switching by replicating the phase transition using the Joule heating and/or an electric field.

Figure 5(a) displays the FMR frequency f_0 determined from the VNA-FMR measurements as a function of the applied out-of-plane field $\mu_0 H$. For all MTJ films, the f_0 linearly increases with increasing $\mu_0 H$; thus, one can estimate from the linear dependence the saturation field H_k as well as PMA energy density $K_u \ (= M_s H_k/2)$. Figure 5(b) summarizes the T_a dependence of K_u for the MTJ films with different t. Regardless of t, K_u maximizes at around $T_a = 250 - 300°C$, and the largest K_u of 0.2 MJ/m^3 is achieved for
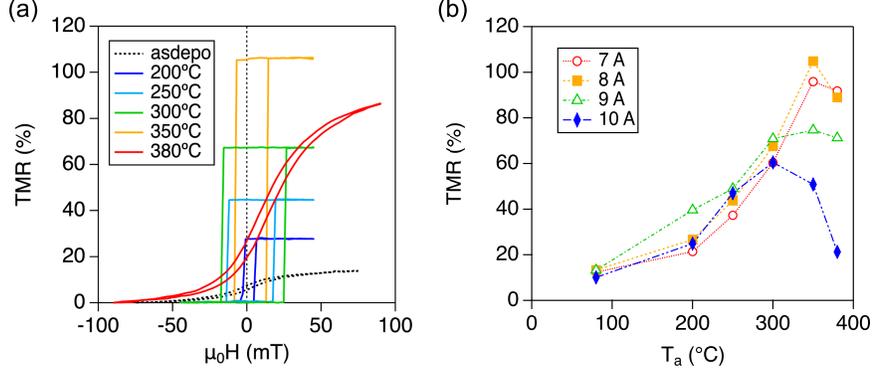
FIG. 6. CIPT measurement results: (a) TMR as function of applied out-of-plane field. (b) TMR as function of T_a.

$T_a = 300°C$ with $t = 0.7$ nm. Although this K_u value is smaller than that reported for MgO/CoFeB/Mo/CoFeB/MgO [30, 37] and Mo buffer/CoFeB/MgO multilayers [38–40], it is comparable to the standard Ta buffer/CoFeB/MgO junctions [10, 35].

Finally, we discuss the TMR characteristics of the Co_3Mn/Mo/CoFeB MTJ films determined from CIPT measurements under an out-of-plane magnetic field. Figure 6(a) displays the TMR curves obtained from the Co_3Mn (0.8 nm)/Mo (0.3 nm)/CoFeB (0.6 nm) MTJ films annealed at various T_a. In accordance with the VSM and FMR measurement results, square-shaped TMR curves, which represent the switching of the perpendicularly magnetized Co_3Mn/Mo/CoFeB free layer are obtained for $T_a = 200 - 350°C$. The Co_3Mn/Mo/CoFeB MTJ film exhibits a large TMR ratio of over 100% after annealing at $T_a = 350°C$. Figure 6(b) displays the T_a dependence of the TMR ratio determined from the CIPT measurement. The largest TMR of 105% is obtained for the Co_3Mn (0.8 nm)/Mo (0.3 nm)/CoFeB (0.6 nm) MTJ film annealed at $T_a = 350°C$. Although this TMR ratio is smaller than that reported for an in-plane-magnetized MTJ using epitaxially grown bcc-Co_3Mn electrodes [22, 23], it should be stressed that we obtained a large TMR ratio of over 100% in *perpendicularly-magnetized* MTJ films using *polycrystalline* Co_3Mn electrodes. Note that the smaller TMR for the MTJ films consisting of 9- and 10-Å-thick Co_3Mn films is due to the unsaturated magnetic moment in the Co_3Mn/Mo/CoFeB layer with insufficient PMA. Further enhancements in the TMR as well as PMA will be readily achieved by improving the flatness of the bottom electrode.

8

IV. SUMMARY

To summarize, we studied the magnetic and electrical transport properties of MTJ films consisting of $Co_3Mn/Mo/CoFeB$ multilayers prepared on a polycrystalline electrode. The $CoMn_3/Mo/CoFeB$ multilayers exhibited remarkable PMA and a fairly large K_u of 0.2 MJ/m^3 was achieved after annealing at $T_a = 300°C$. A TMR ratio of 105% was also obtained for perpendicularly magnetized $Co_3Mn/Mo/CoFeB$ MTJ films. These experimental results will contribute to the development of advanced MRAMs including voltage-controlled MRAM and SOT-MRAM.

[1] H. Yoda, T. Kishi, T. Nagase, M. Yoshikawa, K. Nishimata, E. Kitagawa, T. Daibou, M. Amano, N. Shimomura, S. Takahashi, T. Kai, M. Nakayama, H. Aikawa, S. Ikegawa, M. Nagamine, J. Ozeki, S. Mizukami, M. Oogane, Y. Ando, S. Yuasa, K. Yakushiji, H. Kubota, Y. Suzuki, Y. Nakatani, T. Miyazaki, and K. Ando, "High efficient spin transfer torque writing on perpendicular magnetic tunnel junctions for high density mrams," Curr. Appl. Phys. **10**, e87 (2010).

[2] D.C. Worledge, G. Hu, David W. Abraham, P.L. Trouilloud, and S. Brown, "Development of perpendicularly magnetized Ta—CoFeB—MgO-based tunnel junctions at ibm," J. Appl. Phys. **115**, 172601 (2014).

[3] K. Ando, S. Fujita, J. Ito, S. Yuasa, Y. Suzuki, Y. Nakatani, T. Miyazaki, and H. Yoda, "Spin-transfer torque magnetoresistive random-access memory technologies for normally off computing," J. Appl. Phys. **115**, 172607 (2014).

[4] L. Thomas, G. Jan, J. Zhu, H. Liu, Y.-J. Lee, S. Le, R.-Y. Tong, K. Pi, Y.-J. Wang, D. Shen, R. He, J. Haq, J. Teng, V. Lam, K. Huang, T. Zhong, T. Torng, and P.-K. Wang, "Perpendicular spin transfer torque magnetic random access memories with high spin torque efficiency and thermal stability for embedded applications," J. Appl. Phys. **115**, 172615 (2014).

[5] S. S. P. Parkin, C. Kaiser, A. Panchula, P. M. Rice, B. Hughes, M. Samant, and S.-H. Yang, "Giant tunneling magnetoresistance at room tempereature with MgO (100) tunnel barriers," Nat. Mater. **3**, 862 (2004).

[6] S. Yuasa, T. Nagahama, A. Fukushima, Y. Suzuki, and K. Ando, "Giant room-temperature magnetoresistance in single-crystal Fe/MgO/Fe magnetic tunnel junctions," Nat. Mater. **3**, 868 (2004).

[7] D.D. Djayaprawira, K. Tsunekawa, M. Nagai, H. Maehara, S. Yamagata, N. Watanabe, S. Yuasa, Y. Suzuki, and K. Ando, "230% room-temperature magnetoresistance in CoFeB/MgO/CoFeB magnetic tunnel junctions," Appl. Phys. Lett. **86**, 092502 (2005).

[8] T. Shinjo, S. Hine, and T. Takada, "Mössbauer spectra of ultrathin Fe films coated by MgO," J. de Phys. **40**, C2–86 (1979).

[9] S. Yakata, H. Kubota, Y. Suzuki, K. Yakushiji, A. Fukushima, S. Yuasa, and K. Ando, "Influence of perpendicular magnetic anisotropy on spin-transfer switching current in CoFeB/MgO/CoFeB magnetic tunnel junctions," J. Appl. Phys. **105**, 07D131 (2009).

[10] S. Ikeda, K. Miura, H. Yamamoto, K. Mizunuma, H. D. Gan, M. Endo, S. Kanai, J. Hayakawa, F. Matsukura, and H. Ohno, "A perpendicular-anisotropy CoFeB-MgO magnetic tunnel junction," Nat. Mater. **9**, 721 (2010).

[11] H. Kubota, S. Ishibashi, T. Saruya, T. Nozaki, A. Fukushima, K. Yakushiji, K. Ando, Y. Suzuki, and S. Yuasa, "Enhancement of perpendicular magnetic anisotropy in FeB free layers using a thin MgO cap layer," J. Appl. Phys. **111**, 07C723 (2012).

[12] J. Mathon and A. Umerski, "Theory of tunneling magnetoresistance of an epitaxial Fe/MgO/Fe (001) junction," Phys. Rev. B **63**, 220403 (2001).

[13] W. H. Butler, X.-G. Zhang, T. C. Schulthess, and J. M. MacLaren, "Spin-dependent tunneling conductance of Fe—MgO—Fe sandwiches," Phys. Rev. B **63**, 054416 (2001).

[14] H. X. Yang, M. Chshiev, B. Dieny, J. H. Lee, A. Manchon, and K. H. Shin, "First-principles investigation of the very large perpendicular magnetic anisotropy at Fe—MgO and Co—MgO interfaces," Phys. Rev. B **84**, 054401 (2011).

[15] J. Okabayashi, J. W. Koo, H. Sukegawa, S. Mitani, Y. Takagi, and T. Yokoyama, "Perpendicular magnetic anisotropy at the interface between ultrathin Fe film and MgO studied by angular-dependent X-ray magnetic circular dichroism," Appl. Phys. Lett. **105**, 122408 (2014).

[16] A. Manchon, J. Železný, I. M. Miron, T. Jungwirth, J. Sinova, A. Thiaville, K. Garello, and P. Gambardella, "Current-induced spin-orbit torques in ferromagnetic and antiferromagnetic systems," Rev. Mod. Phys. **91**, 035004 (2019).

[17] I. M. Miron, K. Garello, G. Gaudin, P.-J. Zermatten, M. V. Costache, S. Auffret, S. Bandiera, B. Rodmacq, A. Schuhl, and P. Gambardella, "Perpendicular switching of a single ferromagnetic layer induced by in-plane current injection," Nature **476**, 189 (2011).

[18] L. Liu, C.-F. Pai, Y. Li, H. W. Tseng, D. C. Ralph, and R. A. Buhrman, "Spin-torque switching with the giant spin hall effect of tantalum," Science **336**, 555 (2012).

[19] T. Nozaki, T. Yamamoto, S. Miwa, M. Tsujikawa, M. Shirai, S. Yuasa, and Y. Suzuki, "Recent progress in the voltage-controlled magnetic anisotropy effect and the challenges faced in developing voltage-torque mram," Micromachines **10**, 327 (2019).

[20] Y. Shiota, T. Nozaki, F. Bonell, S. Murakami, T. Shinjo, and Y. Suzuki, "Induction of coherent magnetization switching in a few atomic layers of FeCo using voltage pulses," Nat. Mater. **11**, 39 (2012).

[21] S. Kanai, M. Yamanouchi, S. Ikeda, Y. Nakatani, F. Matsukura, and H. Ohno, "Electric field-induced magnetization reversal in a perpendicular-anisotropy CoFeB-MgO magnetic tunnel junction," Appl. Phys. Lett. **101**, 122403 (2012).

[22] K. Kunimatsu, T. Tsuchiya, T. Roy, K. Elpjick, T. Ichinose, M. Tsujikawa, A. Hirohata, M. Shirai, and S. Mizukami, "Fabrication of magnetic tunnel junctions with a metastable bcc Co_3Mn disordered alloy as a bottom electrode," Jpn. J. Appl. Phys. **58**, 080908 (2019).

[23] K. Kunimatsu, T. Tsuchiya, T. Roy, K. Elpjick, T. Ichinose, M. Tsujikawa, A. Hirohata, M. Shirai, and S. Mizukami, "Magnetic tunnel junctions with metastable bcc Co_3Mn electrodes," Appl. Phys. Express **13**, 083007 (2020).

[24] D. Wu, G. L. Liu, C. Jing, Y. Z. Wu, D. Loison, G. S. Dong, and X. F. Jin, "Magnetic structure of $Co_{1-x}Mn_x$ alloys," Phys. Rev. B **63**, 214403 (2001).

[25] Y. U. Idzerda, H. Bhatkar, and E. Arenholz, "Moment mapping of body-centered-cubic Fe_xMn_{1-x} alloy films on MgO(001)," J. Appl. Phys. **117**, 17A721 (2015).

[26] R. J. Snow, H. Bhatkar, A. T. N'Diaye, E. Arenholz, and Y. U. Idzerda, "Enhanced moments in bcc $Co_{1-x}Mn_x$ on MgO(001)," J. Magn. Magn. Mater. **419**, 490 (2016).

[27] R. J. Snow, H. Bhatkar, A. T. N'Diaye, E. Arenholz, and Y. U. Idzerda, "Large moments in bcc $Fe_xCo_yMn_z$ ternary alloy thin films," Appl. Phys. Lett. **112**, 072403 (2018).

[28] K. Yakushiji, A. Sugihara, A. Fukushima, H. Kubota, and S. Yuasa, "Very strong antiferromagnetic interlayer exchange coupling with iridium spacer layer for perpendicular magnetic tunnel junctions," Appl. Phys. Lett. **110**, 092406 (2017).

[29] D. C. Worledge and P. L. Trouilloud, "Magnetoresistance measurement of unpatterned magnetic tunnel junction wafers by current-in-plane tunneling," Appl. Phys. Lett. **83**, 84 (2005).

[30] H. Cheng, J. Chen, S. Peng, B. Zhang, Z. Wang, D. Zhu, K. Shi, S. Eimer, X. Wang, Z. Guo, Y. Xu, D. Xiong, K. Cao, and W. Zhao, "Giant perpendicular magnetic anisotropy in Mo-based double-interface free layer structure for advanced magnetic tunnel junctions," Adv. Electron. Mater. **6**, 2000271 (2020).

[31] S. Tamaru, T. Yamamoto, T. Onuma, N. Kikuchi, and S. Okamoto, "Development of a high-sensitivity VNA-FMR spectrometer with field modulation detection and its application to magnetic characterization," Electron. Comm. Jpn **104**, e12320 (2021).

[32] P. H. Dederichs, R. Zeller, H. Akai, and H. Ebert, "Ab-initio calculations of the electronic structure of impurities and alloys of ferromagnetic transition metals," J. Magn. Magn. Mater. **100**, 241 (1991).

[33] T. Nozaki, M. Endo, M. Tsujikawa, T. Yamamoto, T. Nozaki, M. Konoto, H. Ohmori, Y. Higo, H. Kubota, A. Fukushima, M. Hosomi, M. Shirai, , Y. Suzuki, and S. Yuasa, "Voltage-controlled magnetic anisotropy in an ultrathin Ir-doped Fe layer with a CoFe termination layer," APL Mater. **8**, 011108 (2020).

[34] T. Yamamoto, T. Nozaki, H. Imamura, Y. Shiota, S. Tamaru, K. Yakushiji, H. Kubota, A. Fukushima, Y. Suzuki, and S. Yuasa, "Improvement of write error rate in voltage-driven magnetization switching," J. Phys. D: Appl. Phys. **52**, 164001 (2019).

[35] T. Yamamoto, T. Nozaki, K. Yakushiji, S. Tamaru, H. Kubota, A. Fukushima, and S. Yuasa, "Perpendicular magnetic anisotropy and its voltage control in MgO/CoFeB/MgO junctions with atomically thin Ta adhesion layers," Acta. Mater. **216**, 117097 (2021).

[36] K. Z. Suzuki, S. Kimura, H. Kubota, and S. Mizukami, "Magnetic tunnel junctions with a nearly zero moment manganese nanolayer with perpendicular magnetic anisotropy," ACS

Appl. Mater. Interfaces **10**, 43305 (2018).

[37] T. Yamamoto, T. Ichhinose, J. Uzuhashi, T. Nozaki, T. Ohkubo, K. Yakushiji, S. Tamaru, H. Kubota, A. Fukushima, K. Hono, and S. Yuasa, "Perpendicular magnetic anisotropy and its voltage control in MgO/CoFeB/Mo/CoFeB/MgO junctions," J. Phys. D: Appl. Phys. **55**, 275003 (2022).

[38] T. Liu, Y. Zhang, J. W. Cai, and H. Y. Pan, "Thermally robust Mo/CoFeB/MgO trilayers with strong perpendicular magnetic anisotropy," Sci. Rep. **4**, 5895 (2014).

[39] H. Almasi, D.Reifsnyder Hickey, T. Newhouse-lllige, M. Xu, M.R. Rosales, S. Nahar, J.T. Held, K.A. Mkhoyan, and W.G. Wang, "Enhanced tunneling magnetoresistance and perpendicular magnetic anisotropy in Mo/CoFeB/MgO magnetic tunnel junctions," Appl. Phys. Lett. **106**, 222409 (2015).

[40] B. Fang, X. Zhang, B.S. Zhang, Z.M. Zeng, and J.W. Cai, "Tunnel magnetoresistance in thermally robust Mo/CoFeB/MgO tunnel junction with perpendicular magnetic anisotropy," AIP Advances **5**, 067116 (2015).